Published in final edited form as:
J Comp Neurol. 2011 February 1; 519(2): 358–375. doi:10.1002/cne.22523.

Topography and Morphology of the Inhibitory Projection From Superior Olivary Nucleus to Nucleus Laminaris in Chickens (Gallus gallus)

KATHRYN M. TABOR[1,2], **RACHEL O.L. WONG**[1,2,3], and **EDWIN W. RUBEL**[1,2,4,5]

[1]Neurobiology and Behavior Graduate Program, University of Washington, Seattle, Washington 98195-7923

[2]Virginia Merrill Bloedel Hearing Research Center, University of Washington, Seattle, Washington 98195-7923

[3]Department of Biological Structure, University of Washington, Seattle, Washington 98195-7923

[4]Department of Physiology and Biophysics, University of Washington, Seattle, Washington 98195-7923

[5]Department of Otolaryngology –HNS, University of Washington, Seattle, Washington 98195-7923

Abstract

The avian nucleus laminaris (NL) is involved in computation of interaural time differences (ITDs) that encode the azimuthal position of a sound source. Neurons in NL are bipolar, with dorsal and ventral dendritic arbors receiving input from separate ears. NL neurons act as coincidence detectors that respond maximally when input from each ear arrives at the two dendritic arbors simultaneously. Computational and physiological studies demonstrated that the sensitivity of NL neurons to coincident inputs is modulated by an inhibitory feedback circuit via the superior olivary nucleus (SON). To understand the mechanism of this modulation, the topography of the projection from SON to NL was mapped, and the morphology of the axon terminals of SON neurons in NL was examined in chickens (Gallus gallus). In vivo injection of AlexaFluor 568 dextran amine into SON demonstrated a coarse topographic projection from SON to NL. Retrogradely labeled neurons in NL were located within the zone of anterogradely labeled terminals, suggesting a reciprocal projection from SON to NL. In vivo extracellular physiological recording further demonstrated that this topography is consistent with tonotopic maps in SON and NL. In addition, three-dimensional reconstruction of single SON axon branches within NL revealed that individual SON neurons innervate a large area of NL and terminate on both dorsal and ventral dendritic arbors of NL neurons. The organization of the projection from SON to NL supports its proposed functions of controlling the overall activity level of NL and enhancing the specificity of frequency mapping and ITD detection.

Indexing terms

auditory brainstem; axonal projection; γ-aminobutyric acid (GABA); interaural time difference (ITD); tonotopic organization

*Correspondence to: Edwin W Rubel, University of Washington, Box 357923, Seattle, Washington 98195-7923. rubel@uw.edu.

Additional Supporting Information may be found in the online version of this article.

Common components of neuronal networks in the central nervous system include long-distance excitatory projections and local inhibitory connections. In addition, inhibition can also be provided by long-range connections between separate nuclei, such as the GABAergic connection from the deep cerebellar nucleus to the inferior olive (Hesslow, 1986; Nelson et al., 1989) and the GABAergic projections from diverse cell populations in the caudal diencephalon and brainstem to the superior colliculus (Appell and Behan, 1990). However, little is known about how long-range inhibitory projections are organized. In the auditory system, a few inhibitory long-range pathways have been studied, including 1) the GABAergic aural dominance bands in the inferior colliculus arising from bilateral projections of the dorsal nucleus of the lateral lemniscus in cat (DNLL; Shneiderman et al., 1988); 2) the well-described precise tonotopic connection from the medial nucleus of the trapezoid body (MNTB) to the lateral superior olive in mammals (LSO; Boudreau and Tsuchitani, 1968; Sanes and Rubel, 1988); and 3) the GABAergic projection from the superior olivary nucleus (SON) to nucleus laminaris (NL) in the chicken brainstem (Lachica et al., 1994; Yang et al., 1999; Burger et al., 2005). The SON projection to NL provides an opportunity to study the organization of inhibitory input in a system in which the excitatory circuit is precisely organized and well characterized. Additionally, understanding the organization of SON inhibition will provide insight into the role of NL neurons in azimuth sound localization. Here, we investigate the topography of the GABAergic projection from SON to NL.

Interaural time differences (ITDs), the submillisecond differences in the arrival time of sound to the two ears, are a critical cue for binaural localization of sound sources. The avian NL, similar to the mammalian medial superior olive (MSO), is the first neural center to receive excitatory input from both ears. The chicken NL is composed of a compact monolayer of bitufted neurons with segregated dorsal and ventral dendrites. Excitatory input from either the ipsilateral or the contralateral ear is relayed in a phase-locked manner through nucleus magnocellularis (NM) and conveyed to the dorsal or ventral dendritic arbor, respectively (Parks and Rubel, 1975; Smith and Rubel, 1979; Young and Rubel, 1983). Individual NL neurons are sensitive to changes in ITDs, responding maximally when input from the ipsilateral and contralateral NM arrives at the two dendritic arbors simultaneously (Carr and Konishi, 1990; Overholt et al., 1992). In addition, NL is characterized by systematic shifts of frequency representation, tonotopy, along its rostromedial to caudolateral axis (Rubel and Parks, 1975). Orthogonal to its tonotopic map, NL is arranged by preferred ITD such that neighboring neurons have adjacent receptive fields along the azimuth (Parks and Rubel, 1975; Young and Rubel, 1983, 1986; Köppl and Carr, 2008).

A fundamental requirement for NL neurons to localize sound effectively is to remain sensitive to ITDs across a large dynamic range of firing rates of their inputs. The firing rate of NM fibers increases threefold or more with increasing sound level (Warchol and Dallos, 1990). One mechanism that preserves ITD sensitivity in NL across sound levels is inhibitory feedback (Nishino et al., 2008). GABAergic inhibitory inputs are abundant on the cell body as well as both dorsal and ventral dendritic lamina of NL (Carr et al., 1989; Code et al., 1989). The inhibitory input arises from a small population of interneurons in the surrounding neuropil (von Bartheld et al., 1989) and a prominent projection from the ipsilateral SON (Lachica et al., 1994; Yang et al., 1999; Burger et al., 2005). SON receives excitatory input from the ipsilateral NL and nucleus angularis (NA) and provides inhibition to the ipsilateral NL, NM, and NA (Lachica et al., 1994; Yang et al., 1999; Monsivais et al., 2000; Burger et al., 2005). Using a computational model of the avian auditory brainstem network, Dasika and colleagues (2005) demonstrated that sound-level-dependent feedback inhibition from the SON can significantly expand the dynamic range of the avian ITD coding system and improve ITD sensitivity.

Individual SON neurons project to multiple ipsilateral target nuclei and thus provide an interaction between the auditory pathways specialized for processing temporal features (NM to NL) and the pathways that process other aspects of sound (Burger et al., 2005). In addition, a separate population of SON neurons projects to the contralateral SON (Burger et al., 2005), which has been suggested to serve to decrease the effects of level imbalances to the two sides (Burger et al., 2005).

The physiological properties of the SON allow these neurons to integrate inputs over long time periods and to respond to the overall activity level of their inputs, instead of encoding precise temporal information about the stimulus structure. Compared with NM neurons, chicken SON neurons show poor phase locking and relatively long time constants and excitatory postsynaptic potential (EPSP) durations (Lachica et al., 1994; Yang et al., 1999; Kuo et al., 2009). Furthermore, direct stimulation of the SON evokes a GABA-mediated inhibition in NL neurons lasting on the order of tens to hundreds of milliseconds (Hyson et al., 1995; Funabiki et al., 1998; Yang et al., 1999; Monsivais et al., 2000; Lu and Trussell, 2001; Monsivais and Rubel, 2001), in contrast to the rapid glutamatergic responses (Raman et al., 1994). In NL, GABAergic input from the SON has been shown to reduce the amplitude and shorten the glutamatergic EPSPs, which may facilitate coincidence detection of the bilateral excitatory inputs (Pena et al., 1996; Funabiki et al., 1998; Yang et al., 1999). This slow inhibition of the glutamatergic response by GABAergic input is consistent with the presumed role of the SON in regulating the gain of the network in order to maintain temporal sensitivity in NL, particularly over variations in sound level.

Although physiological and computational studies have established the critical role of inhibition in ITD coding, the neuronal mechanisms remain unknown. Is the SON regulating NL in a frequency-specific manner or an ITD-specific manner? Is the SON-NL loop homotopic, such that an NL neuron receives inhibitory feedback from the same SON neurons to which it projects? Are SON arborizations confined to specific laminae in NL, suggesting independent regulation of input from each ear within this nucleus? By using in vivo anterograde and retrograde tract tracing methods, the current study examined the topography of the projection from SON to NL and determined the detailed morphology of SON terminals within NL. Our observations also raise the possibility of tonotopic representation in SON.

MATERIALS AND METHODS

White leghorn hatchlings at postnatal days 4–6 were used for all experiments. All procedures were carried out in accordance with the National Institutes of Health Guide for the care and use of laboratory animals and were approved by the University of Washington Institutional Animal Care and Use Committee. All efforts were made to minimize pain or discomfort of the animals and to minimize animal numbers.

Surgery preparation

Chickens were anesthetized with an intramuscular injection of 40 mg/kg ketamine and 12 mg/kg xylazine. Throughout recording and injections, the animal's temperature was maintained at 40°C using a heating pad. The head was fixed to a head holder, and a metal rod was attached to the top of the cranium with dental cement. The skull was exposed, and a hole was made above the cerebellum.

In vivo recordings

Free-field sound stimuli were presented, and the sound pressure level was calibrated at the beginning of each experiment. The maximum sound intensity was 110 dB SPL and the

sound frequency range was 100–6,000 Hz. Sound calibration and electrophysiological recordings were made in an electrically shielded, double-walled, sound-attenuated room. Acoustic stimuli were either pure-tone or white-noise pulses (200 msec duration, 2 msec rise and fall time for a triangular envelope, 3 pulses/second). The recording electrode was a glass micropipette (2–5 MΩ) filled with 5 mM AlexaFluor 568 dextran (D22913; Invitrogen, Eugene, OR) in 3 M sodium acetate. The recording electrode was inserted vertically 1.8–2.0 mm lateral to the midline and 0–0.5 mm rostral to the middorsal sinus. The SON was located by monitoring neuronal responses to a white-noise stimulus (80 dB SPL) while lowering the electrode into the brainstem using a motor driven micromanipulator (model PMC100; Newport, Irvine, CA). Neuronal action potentials were recorded extracellularly with a neuroprobe amplifier (model 1600; A-M Systems, Carlsborg, WA) and bandpass filtered between 80 Hz and 10 kHz (two-pole). Data were collected at 50 kHz sampling frequency with 12-bit resolution. Customized software (SPIKE; B. Warren, University of Washington, Seattle), written in Python, controlled sound presentation and data acquisition.

After isolating a unit or multiunit cluster from background noise, the best frequency (BF) was obtained. The BF was defined as the sound frequency, presented for 200 msec at 70 dB SPL, that elicited the greatest spike rate. Each stimulus was presented 20–30 times in a randomized sequence. For six cases, we obtained a frequency tuning curve to a series of sound frequencies (15–25 frequencies at logarithmic intervals between 0.1 and 6 kHz, 3 pulses/second; Fig. 1). Firing threshold was defined as the sound intensity that induced spiking greater than 2 SD above the spontaneous firing rate. Characteristic frequency (CF) was defined as the frequency with the lowest threshold. Spike sorting and analysis of frequency tuning curves were performed using customized software written by David M. Schneider (Columbia University, New York, NY) in MatLab (Mathworks; Natick, MA).

In vivo tracer injection

After the BF of a recording site had been determined, 100–500 nl of AlexaFluor 568 dextran was injected using a pressure device (PicoSpritzer III; General Valve, Fairfeild, NJ), followed by ionophoresis (positive current, 250 nA for 15–20 minutes). In early experiments, we observed that the combination of pressure and current injection methods resulted in increased transport of tracer to the distal axonal processes compared with the results of using either method alone. It also appeared that short-duration pressure pulses (<20 msec) resulted in relatively more anterograde labeling whereas longer duration pressure pulses (>100 msec) resulted in more retrogradely labeled NL neurons. After injection, the micropipette was retracted, the wound was closed, and the animal was allowed to recover.

Immunohistochemical staining

After a survival time of 2 days, animals were anesthetized with ketamine and xylazine and transcardially perfused with 0.9% saline, followed by chilled 4% paraformaldehyde (PFA) in phosphate buffer (0.1 M, pH 7.4). The brains were removed from the skull and postfixed overnight in PFA at 4°C.

Microtubulin-associated protein 2 (MAP2), glutamate decarboxylase 65 (GAD65), and gephyrin were immunolabeled using a procedure described by Wang and Rubel (2008). Briefly, brainstems were cut coronally at 60 or 300 μm using a Vibratome (TPI, St. Louis, MO), and sections were collected in phosphate-buffered saline (PBS; 0.1 M, pH 7.4). Free-floating sections were incubated with primary antibody solutions diluted 1:1,000 in PBS with 0.3% Triton X-100 and 5% normal goat serum overnight at 4°C, followed by incubation with AlexaFluor secondary antibodies (1:200; Invitrogen) for 2 hours at room temperature.

After immunohistochemistry, tissue sections were dehydrated in a series of ethanol steps and placed into a clearing solution (3:5 mixture of benzyl benzoate and methyl salicylate) to increase the optical transparency of fluorescently labeled tissue slices and to allow confocal images to be collected from the entire depth of the tissue slice (MacDonald and Rubel, 2008).

Antibody characterization

See Table 1 for a list of all antibodies used.

MAP2—Mouse anti-MAP2 monoclonal antibody (MAB3418; lot LV1486526; clone AP20; Chemicon, Temecula, CA) was raised against bovine brain MAP2 (aa 997–1332). The antibody was characterized by Western blot analysis, which showed that this antibody stains high-molecular-weight MAP2 isoforms in adult rat of approximately 300 kD (manufacturer's technical information; Matsunaga et al., 1999). MAP2 associates with microtubules, neurofilaments, and actin filaments and is confined to neuronal cell bodies and dendrites, although small amounts were shown to exist in some axons (Caceres et al., 1984). Our staining results from chicken NL produced a pattern of MAP2 immunoreactivity similar to that described from previous studies (Wang and Rubel, 2008).

GAD65—Polyclonal anti-GAD65 (AB5082; lot LV1580833; Millipore, Billerica, MA) was raised in rabbit against human GAD65 from baculovirus-infected cells. According to the manufacturer's product information, this antibody reacts strongly with GAD65-containing nerve terminals and recognizes a 65-kD protein corresponding to GAD65 by Western blot of mouse brain extract. GAD65 is responsible for catalyzing the production of GABA from L-glutamic acid and is localized to the presynaptic cell membrane. The GAD65 immunolabeling pattern we observed in chicken NL is similar to the distribution pattern previously described for GABAergic synapses in chicken and owl NL; GAD65-positive puncta were located throughout NL and appeared densely distributed on the cell body and proximal dendritic laminae (Carr et al., 1989; Code et al., 1989; Code and Churchill, 1991; Nishino et al., 2008).

Gephyrin—Mouse monoclonal antigephyrin (147011; lot 147011/21; clone mAB7a; Synaptic Systems, Goettingen, Germany) was raised against purified rat gephyrin. By Western blot, this antibody stains the brain-specific 93-kD splice variant and was shown to detect the N-terminus of gephyrin (manufacturer's technical information; Pfeiffer et al., 1984). Gephyrin is a postsynaptic scaffolding protein essential for synaptic clustering of inhibitory neurotransmitter receptors. Our staining results from chicken NL produced a pattern of gephyrin immunolabeling similar to the pattern of GAD65 immunostaining (see Fig. 9A) and the distribution pattern previously described for GABAergic synapses in chicken NL (Code et al., 1989; Code and Churchill, 1991; Nishino et al., 2008).

Fluorescence microscopy

Slices were imaged with an Olympus Fluoview FV300 confocal microscope (Tokyo, Japan) with ×25 (NA 0.8; oil) or ×60 (NA 1.4; oil) objectives. To determine the overlap of AlexaFluor 568 dextran and anti-GAD65 labeling, single optical planes (0.594 μm) of confocal images were analyzed offline in MetaMorph (Molecular Devices; Sunnyvale, CA) and Amira (Mercury Systems; Chelmsford, MA) software. Other image data were collected as z-series of images for offline analysis.

Imaging and data analyses

Four analyses were conducted to measure 1) the volume of the fluorescently labeled injection site in SON (n = 16 animals), 2) the distribution of anterogradely labeled axonal terminals in NL (n = 16 animals, 3) the distribution of retrograde labeled cell bodies in NL (n = 17 cells), and 4) the morphology of individual axonal arborizations in NL (n = 5 arborizations). These measurements were performed on three-dimensional reconstructions of the nuclei, labeled terminals and neurons from serial confocal z-stack images containing SON or NL.

Reconstruction

Injection site—Serial z-stack images of the entire ipsilateral SON were aligned by using anatomical markers such as blood vessels and fluorescently labeled processes that crossed successive slices. The borders of an injection site were operationally defined by the coalesced appearance of labeling. Contours were traced around the injection site in the coronal plane at 10-μm intervals. Labeled cell bodies within SON but outside the injection site were observed occasionally and marked individually. Contours were concatenated to reconstruct the injection site volume in Neurolucida Explorer (MBF Bioscience; Williston, VT). The sizes of injection sites were measured based on the reconstructed volumes.

Terminal fields and cell bodies—Serial z-stack images containing NL were aligned by using anatomical markers as described above. Positions of retrogradely labeled cell bodies within the NL were individually marked. The drawings were edited in Adobe Illustrator and Adobe Photoshop software (Adobe Systems, Mountain View, CA). Axon labeling in NL was reconstructed in three dimensions in Amira software. Occasionally we observed sparsely distributed, small satellites of anterograde label. We did not include these small satellites in calculations relating the positions of injections to the positions of terminal arbors. Examples of these small satellites are seen on the 2-kHz line and the 1-kHz line in Figure 2A,B, respectively. With this exception, all voxels included in the reconstructed images were weighted equally to calculate the center of mass of the labeled terminal distributions within NL. The area and tonotopic spread of the terminal labeling were based on planar projections reconstructed for each case.

To compare across animals, labeled terminal fields were transformed to fit a template of the NL planar projection. We represented the labeled terminal field within NL by drawing a contour circumscribing the terminals. Sparsely distributed, small satellites of anterograde label were not included inside this boundary. Transforming planar projections to the template caused a shift in the predicted CF range spanned by the terminal field (<200 Hz) that was less than the standard error of estimate calculated for the linear regression equation (281 Hz; Rubel and Parks, 1975; see below).

Calculating characteristic frequency from location within NL. The CFs of NL neurons were predicted from the linear relationship between CF and the mediolateral and rostrocaudal location in NL (Rubel and Parks, 1975; see Fig. 4A–C): $CF = 0.027r + 0.014m – 0.088$, where CF = predicted CF (in kHz) of the NL neuron, r = caudal-to-rostral percentile position in NL, and m = lateral-to-medial percentile position in NL. This regression analysis provides a robust prediction of the CF in NL and has been extensively used to categorize structural and functional properties of NL neurons and determine cellular and physiological specializations that vary across the tonotopic axis (Smith and Rubel, 1979; Smith et al., 1983; Lippe and Rubel, 1985; Parks et al., 1987; Reyes et al., 1996; Person et al., 2004; Kuba et al., 2005; Yamada et al., 2005; Nishino et al., 2008).

Nuclei borders—To calculate the percentage of SON or NL occupied by labeling, we reconstructed the entire nucleus. We traced the contours of the nucleus based on either background fluorescence or MAP2 immunoreactivity. Contours were traced at 10-μm intervals through coronal sections of the entire nucleus. The reconstructed SON volume was divided by bisecting the mediolateral, dorsoventral, and rostrocaudal dimensions of SON. Only injection sites completely confined to a hemisphere of SON were categorized as medial (n = 8) or lateral (n = 3), dorsal (n = 5) or ventral (n = 4), rostral (n = 4) or caudal (n = 7) and included in the topographic analyses. To analyze the topography of SON projections, labeled terminal distributions in NL were compared between injection site positions in each of these dimensions.

Axonal arborizations—Arborizations of labeled individual SON axonal branches were reconstructed from serial coronal 300-μm sections in Amira software. Cut ends of an axon in one section were connected properly to the corresponding cut ends of the same axon in the successive section. Only axon branches that were well labeled and isolated from other axons were reconstructed.

Image processing

Digital images of selected sections and terminals were acquired using the confocal microscope. Images were further processed in Photoshop to enhance contrast and alter brightness. No corrections were made for tissue shrinkage, because the distribution of labeling, but not the absolute length or volume, was the focus of the current study.

Statistical analyses

Statistical evaluations were made via Mann-Whitney U test, linear regression analysis, and Spearman's ranked correlation coefficient analysis. Values are presented as mean ± SEM. In figures, an asterisk represents a statistical significance of $P < 0.05$.

RESULTS

Data presented in the current paper resulted from small injections of a bidirectional tracer, AlexaFluor 568 dextran amine, into the SON in vivo. The criteria for inclusion of a case in this study were that the injection site resided completely within the boundaries of SON and occupied less than one-eighth of the total volume of SON. Small injection sites were necessary to elucidate whether the SON projections to NL were topographically organized. Among 16 such cases, injection sites were distributed throughout the dorsoventral, rostrocaudal, and mediolateral dimensions of SON. The organization and morphology of the projections from SON to the ipsilateral nucleus laminaris (NL) are the main focus of the current study. Observations and analyses of the labeling outside the ipsilateral NL are not presented.

Topographic organization of the SON-NL projection

In three cases, anterograde labeling occupied more than half of the area of NL (99%, 70%, and 60%), suggesting the existence of a nontopographic projection from SON to the ipsilateral NL (see Fig. 6A). In 13 cases, NL received a topographically organized projection from the ipsilateral SON. In these cases, the ipsilateral NL exhibited a relatively confined distribution of anterograde labeling, which occupied less than half of the area of the nucleus. The anatomical location of anterogradely labeled terminals in NL correlated with the location of the injection site in SON. Figure 2 demonstrates the labeling pattern of six representative cases. In all cases (Fig. 2A–F), the data are presented from the left side of the brain, with the lateral aspect to the left and rostral aspect toward the top of the figure. Within each panel, the location of the injection is shown in a series of coronal sections through SON

arranged from rostral to caudal (left). The distribution of anterograde labeling in NL is shown both in serial coronal sections through NL (center) and on planar projections of NL (right). Planar projections were constructed from the series of coronal sections to show a horizontal view of NL. CFs were calculated as described by Rubel and Parks (1975) and are shown in Figure 2A. BFs of the injection sites presented in Figure 2 ranged from 0.5 to 3.29 kHz. Figure 2A illustrates a case with an injection into the rostrodorsomedial SON. The BF recorded at the injection site in the SON was 0.5 kHz, lower than the CF region of NL spanned by labeled SON axons, 1–2 kHz. The predominant anterograde labeling was located in the caudomedial NL; however, a satellite of labeled axons was located more rostrally and laterally in NL. The observed satellite terminals in NL may result from either the main injection site or the labeled SON neurons whose cell bodies reside outside the main injection site. Figure 2B shows a small injection into the dorsomedial region of SON (BF 1.04 kHz) and anterograde label restricted to the caudal NL. The spatial position and extent of anterograde labeling were similar to those in Figure 2A. Figure 2C illustrates a case with an injection into the caudomedial SON (BF 1.2 kHz). The majority of anterograde label was located in the lateral NL between 1 and 2.5 kHz. In addition, a smaller satellite of labeled terminals was located more caudally in NL. Figure 2D illustrates a case with an injection into the rostrodorsomedial SON, similar to Figure 2A. In this case, the labeled terminal field was broadly distributed across the rostral NL. The BF of the injection site was 1.45 kHz. Figure 2E,F shows two cases with the injection sites (BF 2.0 kHz and 3.29 kHz, respectively) in the ventral SON. Both injections labeled axons innervating the rostral NL, but the case illustrated in Figure 2E showed more extensive labeling, possibly because the injection site, although small, covered more of the dorsoventral extent of SON at its rostral end. The frequency response curves for the cases in Figure 2B,D,E are shown in Figure 1B,E,F, respectively. We were unable to determine whether SON neurons exhibiting inhibitory and excitatory frequency responses have different projection patterns because of the limited number of injections at locations of inhibitory frequency tuning (n = 2) and the multiple SON cells labeled by each injection.

To examine the topography of the SON-NL connections better, we compared the position of anterograde labeling in NL between cases in which injections were confined to one half of the SON. For these analyses, the SON was divided in half along the rostrocaudal, mediolateral, and dorsoventral axes, and all cases in which the injection was limited to any one hemisphere were included in the analyses presented in Figure 3. For each case, a contour circumscribing the labeled terminal field in NL was color coded to indicate the location of the injection site within the SON. Each panel of Figure 3 shows contours of terminal fields from all cases meeting the injection site criteria mapped onto a single planar projection of NL (gray). Distribution of terminal fields arising from injections restricted to either the rostral (n = 4) or the caudal (n = 7) half of SON showed no apparent separation, suggesting a lack of topography between the rostrocaudal axis of SON and anterograde terminals in NL (Fig. 3A). Similarly, extensive overlap of contours of terminal fields resulting from injections into either the medial (n = 8) or thec lateral (n = 3) half of SON suggests no topography between the mediolateral axis of SON and anterograde terminals in NL (Fig. 3B). On the other hand, terminal fields from injections into either the dorsal (n = 5) or the ventral (n = 4) SON appeared reasonably well segregated, indicating a topographic projection from dorsal SON to caudal NL and from ventral SON to rostral NL (Fig. 3C). Figure 4 shows quantification of 1) the relationships between the anatomical position of SON injection sites and the CFs of NL spanned by the labeled terminals (Fig. 4A–C) and 2) the relationships between the locations and BFs of injection sites within SON (Fig. 4D–F). These data are derived from the same cases shown in Figure 3. In Figure 3A–C, the lozenges and squares indicate tonotopic positions of the center of mass of the terminal fields. Bars represent the frequency range of NL innervated by labeled SON axons. Consistently with the illustrations in Figure 3, CFs of NL at the center of terminal fields were not significantly

different between cases with caudal (average of cases: 1.92 ± 0.23 kHz; lozenges) and rostral (2.39 ± 0.38 kHz; squares) SON injections sites (Fig. 4A) or between cases with medial (1.62 ± 0.19 kHz; lozenges) and lateral (2.03 ± 0.36 kHz; squares) injection sites (Fig. 4B). In contrast, projections from the dorsal (lozenges) SON innervated a significantly lower frequency region of NL (1.56 ± 0.31 kHz) than projections from the ventral (squares) SON (2.72 ± 0.06 kHz; P = 0.032, U = 1.5, two-tailed; Fig. 4C). Figure 4D–F shows quantification of the organization of frequency tuning within SON. Lozenges and squares designate BFs at injection sites in SON. The BFs were not significantly different between recordings at caudal (1.46 ± 0.28 kHz) and rostral (1.81 ± 0.58 kHz) injection sites (Fig. 4D) or between BFs recorded from the medial (0.87 ± 0.14 kHz) vs. lateral (1.86 ± 0.71 kHz) SON (Fig. 4E). In contrast, we found a significant difference between the BFs recorded from the dorsal (0.86 ± 0.21 kHz) vs. ventral (2.75 ± 0.30 kHz) SON (P = 0.016, U = 0.00, two-tailed; Fig. 4F).

The results from Figures 3 and 4 indicate the SON-NL projections were topographically organized such that neurons of the ventral SON innervated the rostral NL and neurons of the dorsal SON contacted the caudal NL. In addition, the dorsoventral axis of the SON appeared to be tonotopically organized; SON neurons with higher BFs were located ventrally, and SON neurons with progressively lower BFs were located more dorsally within the nucleus.

To examine further the topographic organization of the SON-NL projection in 15 cases, we ranked the cases by the location of the injection site along the dorsoventral, mediolateral, or rostrocaudal axis of SON. We found significant correlations between the ventral-to-dorsal ranking and the CF at the center of the terminal field (r2 = 0.61, P = 0.0006) and between the lateral-to-medial ranking and the CF at the center of the terminal field (r2 = 0.37, P = 0.016), but not between the rostral-to-caudal ranking and the CF at the center of the terminal field (r2 = 0.03, P = 0.532; Supp. Info. Fig. 1).

Tonotopic organization of the SON-NL projection

To visualize better the relationship between frequency tuning of SON neurons and the location of their axonal arbors in NL, Figure 5A shows contours of SON terminal fields (n = 15) mapped onto a single planar projection of NL (gray). One case was excluded from the analysis because it showed anterograde labeling extending across the entire tonotopic axis in NL and no tonotopicity of the SON-NL projection. The color of the contours represents the BF recorded at the injection site using a color scale (Fig. 5A, left). Terminal fields largely occupied the caudal two-thirds of NL following tracer injections in SON locations with low BFs (Fig. 5A, cool colors). In contrast, terminal fields mostly occupied the rostral two-thirds of NL following injections in locations with high BFs (Fig. 5A, warm colors). Figure 5B shows the BF at the injection sites plotted against the frequency range of NL innervated by anterogradely labeled terminals. The CF of NL at the center of the terminal labeling was correlated with the BF recorded at the injection site in SON (r2 = 0.68, P < 0.001, n = 15). The six representative cases illustrated in Figure 2 are indicated with an asterisk in Figure 5B. The data presented above indicate that the projection from SON to NL is topographically, and tonotopically organized. On the other hand, organization of this inhibitory projection appears to be far less precise than the excitatory pathway from NM to NL (Parks and Rubel, 1975; Young and Rubel, 1983). Although this conclusion agrees with previous findings using retrograde labeling methods (Burger et al., 2005), it could also result from diffusion and uptake of tracer through a much greater volume of SON than we detected. If the extent of the terminal fields in NL was governed largely by the size of the injection site in SON, then there should be a correlation between these parameters. The scatterplots shown in Figure 6 suggest that there was no reliable relationship between the size of the injection sites in SON and the overall area (Fig. 6A) or tonotopic extent (Fig. 6B) of the anterograde labeling in NL. All of the injection sites in SON were relatively small

(less than 12.5% volume of SON), yet the spatial extent of anterograde labeling in the ipsilateral NL varied greatly, ranging from 8% to 99% the area of NL. Therefore, the tonotopic organization of the SON projection to NL was not a reflection of the tracer injection methods.

Distribution of retrogradely labeled NL neurons

In vivo tracing methods used in this study were optimized for anterograde transport of tracer; however, in seven cases, we observed retrogradely labeled NL neurons. Eighty-eight percent (15 of 17) of retrogradely labeled NL neurons were positioned within the anterogradely labeled terminal field. Figure 7 is an image of the intermediate CF region of NL showing a retrogradely labeled NL neuron (open arrowhead) surrounded by labeled SON axonal arbors (solid arrowheads). These observations suggest that NL neurons receive inhibitory input from roughly the same region of SON that they contact.

Morphology of SON axonal arborizations in NL

We confirmed that SON axons innervated the rostrocaudal and mediolateral extent of NL and that these terminals were distributed throughout the dorsal, ventral, and cell body laminae of the nucleus. Figure 8 shows a section through NL double-labeled with AlexaFluor 568 dextran amine (yellow) following an injection into SON, and MAP2 immunolabeling (red) illustrating dendrites and cell bodies of NL neurons. The monolayer arrangement of NL neurons is apparent with the dorsal dendrites above and the ventral dendrites below the cell body lamina. We observed that SON axons enter NL from both the dorsal and the ventral sides and that thin SON axon branches wind through NL, forming large varicosities on all laminae.

SON axonal swellings in NL are GABAergic. In six cases, following in vivo injections labeling SON axons projecting to NL, tissue sections were immunostained against GAD65 to visualize the distribution of GABAergic terminals along the labeled SON axonal arbors. To test the specificity of the GAD65 antibody, we colabeled NL using an antibody against the GABAergic postsynaptic maker gephyrin (Fig. 9A). The evident colocalization of GAD65- and gephyrin-positive puncta suggests that the GAD65 antibody is labeling GABAergic terminals. The merged images in Figure 9D,E show that bouton-like varicosities along the axons colocalized with GAD65 labeling, suggesting that these varicosities were GABAergic terminals. To control for random overlap of GAD65-positive puncta and labeled axonal terminals, the GAD65 image was rotated 90° clockwise before merging with the image of labeled SON axons (Fig. 9F). The GAD65-positive puncta rarely overlapped the labeled SON terminals in the rotated image.

Morphology of individual SON axonal arborizations in NL

The morphology of five isolated SON axonal branches was investigated in greater detail. It is unknown how much of the SON neuron's total axonal arbor was represented by the branches we describe below, because we were not able to trace an axon back to its cell body in SON. However, we were able to follow each SON arbor to a single large-diameter axon outside the NL. Figure 10 shows two representative SON axonal branches innervating high- and low-CF regions of NL. The SON axonal arborizations formed bouton-like axonal swellings across all laminae of NL regardless of whether they innervated the rostral, high-CF region of NL (Fig. 10A) or the caudal, low-CF region of NL (Fig. 10B).

We calculated the CF ranges of NL innervated by individual SON axonal branches. In contrast to excitatory inputs that innervated a narrow frequency band of NL, SON inhibitory inputs ramified across a broad range of the tonotopic axis (312 ± 74 μm, 0.86 ± 0.6 kHz, n = 5). This average distance (312 μm) represents about one-third of the total distance along the

tonotopic axis (Seidl et al., 2010). The spread of SON arborizations across the mediolateral axis varies widely (448 ± 298 μm, n = 5), accounting for over half of this axis on average. Thus, it is likely that single axons ramify broadly within NL.

Burger et al. (2005) used retrograde tracing methods to show that single SON neurons innervate multiple auditory nuclei. We confirmed this finding by observing that individual SON axons formed branches and bouton-like structures within NL and NM (not shown) or NL and NA. Figure 11 shows an SON axon (white) that formed branches and bouton-like swellings through the lateral edge of NL, exited NL, and innervated NA, where it formed an intricate arborization. The borders of nuclei are indicated with dotted lines. The axonal varicosities located in NL and NA are enlarged and presented in Figure 11B,C, respectively. One possibility is that labeled arborizations innervating multiple auditory brainstem nuclei did not necessarily originate from SON neurons but originated from neurons that were retrogradely labeled and sent axon collaterals into NL and NM or NA. On the other hand, no study has reported an axon projection from NA coursing through NL or NM, and NL axons do not send collaterals to NM or NA (Burger et al., 2005). Hence our working hypothesis is that SON axons often project to multiple ipsilateral nuclei in the dorsal brainstem.

DISCUSSION

The aim of these experiments was to understand better the anatomical organization of inhibitory input to the low-frequency sound localization circuit in birds. The present study demonstrates that the GABAergic projection from superior olivary nucleus (SON) to nucleus laminaris (NL) is organized in a broad tonotopic pattern. Single SON axonal arborizations terminate on both dendritic laminae as well as the cell body layer and extend across large regions of NL. The SON-NL feedback loop is homotopic; NL neurons receive inhibitory input from the same region of the SON to which they project. In addition, our data demonstrated that single SON neurons project to multiple ipsilateral nuclei in the auditory brainstem, which is consistent with a previous study (Burger et al., 2005). Below we compare the topographic organization of the SON-NL connection to inhibitory projections in other auditory systems and to the excitatory inputs to NL and discuss functional implications of the SON axonal arbor organization in NL.

Methodological considerations

In this study, the structural patterning of the axonal projection from SON to NL was examined by using in vivo anterograde and retrograde tract tracing methods. In several cases, we were able to isolate and reconstruct axonal arbors that originated from single SON axons. Because the anterograde tracing methods used in this study did not allow the reconstruction of an SON axon from its origin at the soma, the total extent of axonal arbors of single SON neurons could not be determined.

Labeling of axonal terminals in NL following injections into SON was considered to be due to uptake of the tracers by SON neurons, because no other known inputs to NL pass through or nearby SON in chickens. A recent study reported a sparse projection from the ventral nucleus of the lateral lemniscus to NL in zebra finches (Wild et al., 2009, 2010). This projection is not GABAergic, whereas labeled terminals in the current study express GAD65.

Retrogradely labeled neurons in NL may either innervate SON or extend their axons through SON before innervating the lateral lemnisicus and nucleus mesencephalicus lateralis pars dorsalis (Boord, 1968; Conlee and Parks, 1986; Takahashi and Konishi, 1988). However, the possibility of two populations of retrogradely labeled NL neurons does not affect our conclusion that the SON-NL feedback loop is homotopic, because the vast majority of

labeled neurons, regardless of their nature, were found within the anterogradely labeled terminal fields.

Broad topography of the projection from SON to NL

The topography of long-range inhibitory projections has received relatively little attention. Studying the topographic organization of these pathways has provided critical insights into the function of the inhibitory input in these systems. For example, the inhibitory connection from the deep cerebellar nucleus (DCN) to the inferior olive (IO) follows a precise topographic arrangement so that a closed loop is formed among neurons of the IO, DCN, and cerebellar cortex (Hesslow, 1986; Nelson et al., 1989). This arrangement forms independent inhibitory feedback loops that each regulate the background activity of a microzone of Purkinje cells and control of cerebellar learning. We found that, in contrast to the DCN-IO connection, the SON shows a broad pattern of innervation within NL.

Another example of a long-range inhibitory pathway is the commissural projection between the two superior colliculi (SC). This GABAergic projection follows a heterotopic organization. The medial SC contacts neurons in the lateral region of the contralateral SC and the lateral SC projects to the medial contralateral SC (Takahashi et al., 2007). This heterotopic arrangement allows regions of the SC representing upward saccades to inhibit contralateral regions representing downward saccades and visa versa. In contrast, our findings suggest that NL neurons receive inhibitory feedback from SON neurons that they contact. However, based on the methods used in the present study alone, we were unable to determine the total number of SON cells contacting a single NL neuron or to ascertain what portion of these SON neurons receives input from this single NL cell.

The mammalian auditory brainstem possesses well-characterized inhibitory projection pathways. Two well-studied examples are the projection from the medial nucleus of the trapezoid body (MNTB) to the lateral superior olive (LSO; Boudreau and Tsuchitani, 1968; Sanes and Rubel, 1988) and the projection from the MNTB to the medial superior olive (MSO), the mammalian analogue to NL (Grothe and Sanes, 1993, 1994). Both inhibitory pathways are involved in sound localization circuits and show topographic organizations with precision similar to that of the excitatory inputs from cochlear nuclei to LSO and MSO (Werthat et al., 2008). This organization allows neurons in the MSO and LSO to integrate timing information from multiple inputs at specific frequencies. Likewise, in the avian auditory brainstem, the excitatory input from nucleus magnocellularis (NM) to NL shows a precise topography, with narrow terminal arborization orthogonal to the tonotopic dimension (Parks and Rubel, 1975; Young and Rubel, 1983). In stark contrast to the precision of the NM-NL connection; however, we found that GABAergic neurons in small regions of SON innervate extensive territories of NL. In most cases, SON axonal terminations were distributed in a broadly topographic manner; i.e., the ventral SON innervates primarily the rostromedial region of NL, and the dorsal SON neurons innervate mainly the caudolateral NL, but injection sites that appeared to occupy less than one-eighth of SON typically labeled terminal arbors covering 30–60% of the frequency axis of NL. When we were able to trace single SON axons as they entered NL, we found that they traversed about one-third (0.9 ± 0.6 kHz, n = 5) of the tonotopic axis of NL. Our observations suggest that the topography of SON to NL connection is mapped mainly in the dorsoventral axis but not in the rostrocaudal and mediolateral axes. Occasionally, small injection sites labeled axonal terminals that occupied an even larger area of NL, and once even the whole nucleus. Although the cause of this variability remains to be determined, it raises the possibility that the projection from SON to NL contains both nontopographic and broadly topographic projections. The potential functional significance of these projection patterns is discussed below (see under Functional implications of the projection from SON to NL).

Tonotopic relationship of SON and NL

A fundamental organizing principle of auditory regions of the brain is tonotopy, the orderly representation of the sound frequency to which neurons are most sensitive. Tonotopy arises from the coding of frequency along the receptor organ and the topographic organization throughout the ascending auditory pathways. Physiological methods are usually necessary to map the tonotopic organization and frequency tuning of auditory nuclei, but the tonotopy of projections can be studied anatomically when the tonotopic organization of the target structure is known and injections are made at positions where recordings are made.

The precise tonotopic organization of NL in hatchling chickens was quantitatively mapped by Rubel and Parks (1975), and several investigators have used this map to assess other physiological and anatomical properties of this nucleus (see Materials and Methods). Our results demonstrate that, overall, the SON projection to NL shows a tonotopic organization, but the arrangement is considerably less precise than the bilateral excitatory inputs from NM to NL. The complete tonotopic spread of single axon arborizations has not been determined but these small injections along with reconstructions of single axonal branches suggest that some SON axons extend across one to three octaves of the tonotopic dimension of NL.

A better understanding of the affect of coarsely organized inhibition in NL on ITD detection will require detailed tonotopic mapping of the SON. Although the tonotopic organization of the avian SON has not been examined in detail, Moiseff and Konishi (1983) reported a dorsal (low frequency) to ventral (high frequency) tonotopic organization in the barn owl. Our study suggests the existence of a similar tonotopic organization in hatchling chickens. We saw no evidence of a tonotopic representation in the rostrocaudal or mediolateral dimensions; however, these interpretations should be viewed as preliminary until a thorough three-dimensional tonotopic map is published. Organization of individual SON axonal terminals within NL

Occasionally, small injections confined to a subregion of SON produced little overlap of labeled axons and allowed us to reconstruct large terminal branches of individual axons. We observed that individual SON arbors terminate in both the dorsal and the ventral dendritic laminae, as well as the cell body layer of NL, which is consistent with previous tracing and immunohistochemical studies showing that inhibitory terminals are distributed across all laminae of NL (Code et al., 1989; Code and Churchill, 1991; Lachica et al., 1994; Nishino et al., 2008). In contrast, inhibitory synapses in the mammalian MSO appear to be mostly confined to the cell bodies (Clark, 1969; Perkins, 1973; Kapfer et al., 2002).

We also observed that branches from a single SON axon extended across roughly one-third of the distance along the tonotopic axis and half of the mediolateral dimension of NL. The large spread of individual SON axonal branches is thus consistent with the broad topography of the inhibitory projection to NL that we observed.

The SON receives excitatory input from NL and nucleus angularis (NA) and provides inhibition to NL, NA, and NM (Lachica et al., 1994; Yang et al., 1999; Monsivais et al., 2000; Burger et al., 2005). Our reconstructions further showed that individual SON neurons project to both NA and NL or to both NM and NL, corroborating previous conclusions by Burger and colleagues (2005).

Functional implications of the projection from SON to NL

Our results provide insight into the functional role of this inhibitory feedback circuit on frequency mapping and ITD detection. In the majority of cases, we found a broad topographic organization along the tonotopic axis of NL. This organization of inhibition is desirable to enhance the recognition of a target signal among competing background signals

having similar spectral properties, as described by Lewicki (2002). In addition, in a few cases, we found a nontopographic SON-NL projection. This projection pattern may further regulate the overall gain of the NL responses. This arrangement is highly beneficial under conditions of high background noise. The organization of SON input may allow NL to adapt to the overall sound level of the acoustic environment, by resetting the gain of the system to an optimal position on the input–output function. This interpretation is supported by physiological data suggesting that SON neurons integrate inputs over a long time scale and provide relatively long-lasting inhibition to NL neurons (Yang et al., 1999; Monsivais et al., 2000). Our data are consistent with the proposed integrative role of the SON in controlling the gain of the ITD processing system, especially at high sound levels (Burger et al., 2005; Nishino et al., 2008; Nishino and Ohmori, 2009).

We found two SON units that displayed frequency-specific suppression of their spontaneous spike rates. The responses of these two units may be shaped by a strong frequency-specific inhibition from the contralateral SON. This SON-SON projection has been shown previously (Burger et al., 2005).

Supplementary Material

Refer to Web version on PubMed Central for supplementary material.

Acknowledgments

We thank Drs. Paul Philips, Fred Rieke, and Yuan Wang for helpful comments on the manuscript; Mr. Glen MacDonald for imaging advice; Mr. Dale Cunningham for advice on immunohistochemical methods; and Mr. Brandon Warren for help with SPIKE software.

Grant sponsor: National Institute of Deafness and Other Communication Disorders; Grant number: DC03829; Grant number: DC04661; Grant number: DC005361.

LITERATURE CITED

Appell PP, Behan M. Sources of subcortical GABAergic projections to the superior colliculus in the cat. J Comp Neurol. 1990; 302:143–158. [PubMed: 2086611]

Boord RL. Ascending projections of the primary cochlear nuclei and nucleus laminaris in the pigeon. J Comp Neurol. 1968; 133:523–541. [PubMed: 4185132]

Boudreau JC, Tsuchitani C. Binaural interaction in the cat superior olive S segment. J Neurophysiol. 1968; 31:442–454. [PubMed: 5687764]

Burger RM, Cramer KS, Pfeiffer JD, Rubel EW. Avian superior olivary nucleus provides divergent inhibitory input to parallel auditory pathways. J Comp Neurol. 2005; 481:6–18. [PubMed: 15558730]

Caceres A, Binder LI, Payne MR, Bender P, Rebhun L, Steward O. Differential subcellular localization of tubulin and the microtubule-associated protein MAP2 in brain tissue as revealed by immunocytochemistry with monoclonal hybridoma antibodies. J Neurosci. 1984; 4:394–410. [PubMed: 6699682]

Carr CE, Konishi M. A circuit for detection of interaural time differences in the brain stem of the barn owl. J Neurosci. 1990; 10:3227–3246. [PubMed: 2213141]

Carr CE, Fujita I, Konishi M. Distribution of GABAergic neurons and terminals in the auditory system of the barn owl. J Comp Neurol. 1989; 286:190–207. [PubMed: 2794115]

Clark GM. The ultrastructure of nerve endings in the medial superior olive of the cat. Brain Res. 1969; 14:293–305. [PubMed: 5794908]

Code RA, Churchill L. GABA A receptors in auditory brainstem nuclei of the chick during development and after cochlea removal. Hear Res. 1991; 54:281–295. [PubMed: 1657849]

Code RA, Burd GD, Rubel EW. Development of GABA immunoreactivity in brainstem auditory nuclei of the chick: ontogeny of gradients in terminal staining. J Comp Neurol. 1989; 284:504–518. [PubMed: 2768549]

Conlee JW, Parks TN. Origin of ascending auditory projections to the nucleus mesencephalicus lateralis pars dorsalis in the chicken. Brain Res. 1986; 367:96–113. [PubMed: 3697720]

Dasika VK, White JA, Carney LH, Colburn HS. Effects of inhibitory feedback in a network model of avian brain stem. J Neurophysiol. 2005; 94:400–414. [PubMed: 15744007]

Funabiki K, Koyano K, Ohmori H. The role of GABAergic inputs for coincidence detection in the neurones of nucleus laminaris of the chick. J Physiol. 1998; 508:851–869. [PubMed: 9518738]

Grothe B, Sanes DH. Bilateral inhibition by glycinergic afferents in the medial superior olive. J Neurophysiol. 1993; 69:1192–1196. [PubMed: 8492158]

Grothe B, Sanes DH. Synaptic inhibition influences the temporal coding properties of medial superior olivary neurons: an in vitro study. J Neurosci. 1994; 14:1701–1709. [PubMed: 8126564]

Hesslow G. Inhibition of inferior olivary transmission by mesencephalic stimulation in the cat. Neurosci Lett. 1986; 63:76–80. [PubMed: 3005925]

Hyson RL, Reyes AD, Rubel EW. A depolarizing inhibitory response to GABA in brainstem auditory neurons of the chick. Brain Res. 1995; 677:117–126. [PubMed: 7606455]

Kapfer C, Seidl AH, Schweizer H, Grothe B. Experience-dependent refinement of inhibitory inputs to auditory coincidence-detector neurons. Nat Neurosci. 2002; 5:247–253. [PubMed: 11850629]

Köppl C, Carr CE. Maps of interaural time difference in the chicken's brainstem nucleus laminaris. Biol Cybern. 2008; 98:541–559. [PubMed: 18491165]

Kuba H, Yamada R, Fukui I, Ohmori H. Tonotopic specialization of auditory coincidence detection in nucleus laminaris of the chick. J Neurosci. 2005; 25:1924–1934. [PubMed: 15728832]

Kuo SP, Bradley LA, Trussell LO. Heterogeneous kinetics and pharmacology of synaptic inhibition in the chick auditory brainstem. J Neurosci. 2009; 29:9625–34. [PubMed: 19641125]

Lachica EA, Rubsamen R, Rubel EW. GABAergic terminals in nucleus magnocellularis and laminaris originate from the superior olivary nucleus. J Comp Neurol. 1994; 348:403–418. [PubMed: 7844255]

Lewicki MS. Efficient coding of natural sounds. Nat Neurosci. 2002; 5:356–363. [PubMed: 11896400]

Lippe W, Rubel EW. Ontogeny of tonotopic organization of brain stem auditory nuclei in the chicken: implications for development of the place principle. J Comp Neurol. 1985; 237:273–289. [PubMed: 4031125]

Lu T, Trussell LO. Mixed excitatory and inhibitory GABA-mediated transmission in chick cochlear nucleus. J Physiol. 2001; 535:125–131. [PubMed: 11507163]

MacDonald GH, Rubel EW. Three-dimensional imaging of the intact mouse cochlea by fluorescent laser scanning confocal microscopy. Hear Res. 2008; 243:1–10. [PubMed: 18573326]

Matsunaga W, Miyata S, Hashimoto Y, Lin SH, Nakashima T, Kiyohara T, Matsumoto T. Microtubule-associated protein-2 in the hypothalamo-neurohypophysial system: low-molecular-weight microtubule-associated protein-2 in pituitary astrocytes. Neuroscience. 1999; 88:1289–1297. [PubMed: 10336137]

Moiseff A, Konishi M. Binaural characteristics of units in the owl's brainstem auditory pathway: precursors of restricted spatial receptive fields. J Neurosci. 1983; 3:2553–2562. [PubMed: 6655499]

Monsivais P, Rubel EW. Accommodation enhances depolarizing inhibition in central neurons. J Neurosci. 2001; 21:7823–7830. [PubMed: 11567073]

Monsivais P, Yang L, Rubel EW. GABAergic inhibition in nucleus magnocellularis: implications for phase locking in the avian auditory brainstem. J Neurosci. 2000; 20:2954–2963. [PubMed: 10751448]

Nelson BJ, Adams JC, Barmack NH, Mugnaini E. Comparative study of glutamate decarboxylase immunoreactive boutons in the mammalian inferior olive. J Comp Neurol. 1989; 286:514–539. [PubMed: 2778105]

Nishino E, Ohmori H. The modulation by intensity of the processing of interaural timing cues for localizing sounds. Mol Neurobiol. 2009; 40:157–165. [PubMed: 19593674]

Nishino E, Yamada R, Kuba H, Hioki H, Furuta T, Kaneko T, Ohmori H. Sound-intensity-dependent compensation for the small interaural time difference cue for sound source localization. J Neurosci. 2008; 28:7153–7164. [PubMed: 18614685]

Overholt EM, Rubel EW, Hyson RL. A circuit for coding interaural time differences in the chick brainstem. J Neurosci. 1992; 12:1698–1708. [PubMed: 1578264]

Parks TN, Rubel EW. Organization and development of brain stem auditory nuclei of the chicken: organization of projections from n. magnocellularis to n. laminaris. J Comp Neurol. 1975; 164:435–448. [PubMed: 1206128]

Parks TN, Gill SS, Jackson H. Experience-independent development of dendritic organization in the avian nucleus laminaris. J Comp Neurol. 1987; 260:312–319. [PubMed: 3611407]

Pena JL, Viete S, Albeck Y, Konishi M. Tolerance to sound intensity of binaural coincidence detection in the nucleus laminaris of the owl. J Neurosci. 1996; 16:7046–7054. [PubMed: 8824340]

Perkins RE. An electron microscopic study of synaptic organization in the medial superior olive of normal and experimental chinchillas. J Comp Neurol. 1973; 148:387–415. [PubMed: 4354692]

Person AL, Cerretti DP, Pasquale EB, Rubel EW, Cramer KS. Tonotopic gradients of Eph family proteins in the chick nucleus laminaris during synaptogenesis. J Neurobiol. 2004; 60:28–39. [PubMed: 15188270]

Raman IM, Zhang S, Trussell LO. Pathway-specific variants of AMPA receptors and their contribution to neuronal signaling. J Neurosci. 1994; 14:4998–5010. [PubMed: 7913958]

Reyes AD, Rubel EW, Spain WJ. In vitro analysis of optimal stimuli for phase-locking and time-delayed modulation of firing in avian nucleus laminaris neurons. J Neurosci. 1996; 16:993–1007. [PubMed: 8558268]

Rubel EW, Parks TN. Organization and development of brain stem auditory nuclei of the chicken: tonotopic organization of n. magnocellularis and n. laminaris. J Comp Neurol. 1975; 164:411–433. [PubMed: 1206127]

Sanes DH, Rubel EW. The ontogeny of inhibition and excitation in the gerbil lateral superior olive. J Neurosci. 1988; 8:682–700. [PubMed: 3339433]

Seidl AH, Rubel EW, Harris DM. Mechanisms for adjusting interaural time differences to achieve binaural coincidence detection. J Neurosci. 2010; 30:70–80. [PubMed: 20053889]

Shneiderman A, Oliver DL, Henkel CK. Connections of the dorsal nucleus of the lateral lemniscus: an inhibitory parallel pathway in the ascending auditory system? J Comp Neurol. 1988; 276:188–208. [PubMed: 3220980]

Smith DJ, Rubel EW. Organization and development of brain stem auditory nuclei of the chicken: dendritic gradients in nucleus laminaris. J Comp Neurol. 1979; 186:213–239. [PubMed: 447882]

Smith ZD, Gray L, Rubel EW. Afferent influences on brainstem auditory nuclei of the chicken: n. laminaris dendritic length following monaural conductive hearing loss. J Comp Neurol. 1983; 220:199–205. [PubMed: 6315783]

Takahashi M, Sugiuchi Y, Shinoda Y. Commissural mirror-symmetric excitation and reciprocal inhibition between the two superior colliculi and their roles in vertical and horizontal eye movements. J Neurophysiol. 2007; 98:2664–2682. [PubMed: 17728384]

Takahashi TT, Konishi M. Projections of nucleus angularis and nucleus laminaris to the lateral lemniscal nuclear complex of the barn owl. J Comp Neurol. 1988; 274:212–238. [PubMed: 2463287]

von Bartheld CS, Code RA, Rubel EW. GABAergic neurons in brainstem auditory nuclei of the chick: distribution, morphology, and connectivity. J Comp Neurol. 1989; 287:470–483. [PubMed: 2477407]

Wang Y, Rubel EW. Rapid regulation of microtubule-associated protein 2 in dendrites of nucleus laminaris of the chick following deprivation of afferent activity. Neuroscience. 2008; 154:381–389. [PubMed: 18440716]

Warchol ME, Dallos P. Neural coding in the chick cochlear nucleus. J Comp Physiol. 1990; A166:721–734. [PubMed: 2341992]

Werthat F, Alexandrova O, Grothe B, Koch U. Experience-dependent refinement of the inhibitory axons projecting to the medial superior olive. Dev Neurobiol. 2008; 68:1454–1462. [PubMed: 18777566]

Wild JM, Krutzfeldt NO, Kubke MF. Afferents to the cochlear nuclei and nucleus laminaris from the ventral nucleus of the lateral lemniscus in the zebra finch (Taeniopygia guttata). Hear Res. 2009; 257:1–7. [PubMed: 19631727]

Wild JM, Krutzfeldt NO, Kubke MF. Connections of the auditory brainstem in a songbird, Taeniopygia guttata. III. Projections of the superior olive and lateral lemniscal nuclei. J Comp Neurol. 2010; 518:2149–2167. [PubMed: 20394063]

Yamada R, Kuba H, Ishii TM, Ohmori H. Hyperpolarization-activated cyclic nucleotide-gated cation channels regulate auditory coincidence detection in nucleus laminaris of the chick. J Neurosci. 2005; 25:8867–8877. [PubMed: 16192376]

Yang L, Monsivais P, Rubel EW. The superior olivary nucleus and its influence on nucleus laminaris: a source of inhibitory feedback for coincidence detection in the avian auditory brainstem. J Neurosci. 1999; 19:2313–2325. [PubMed: 10066281]

Young SR, Rubel EW. Frequency-specific projections of individual neurons in chick brainstem auditory nuclei. J Neurosci. 1983; 3:1373–1378. [PubMed: 6864252]

Young SR, Rubel EW. Embryogenesis of arborization pattern and topography of individual axons in N. laminaris of the chicken brain stem. J Comp Neurol. 1986; 254:425–459. [PubMed: 3805357]

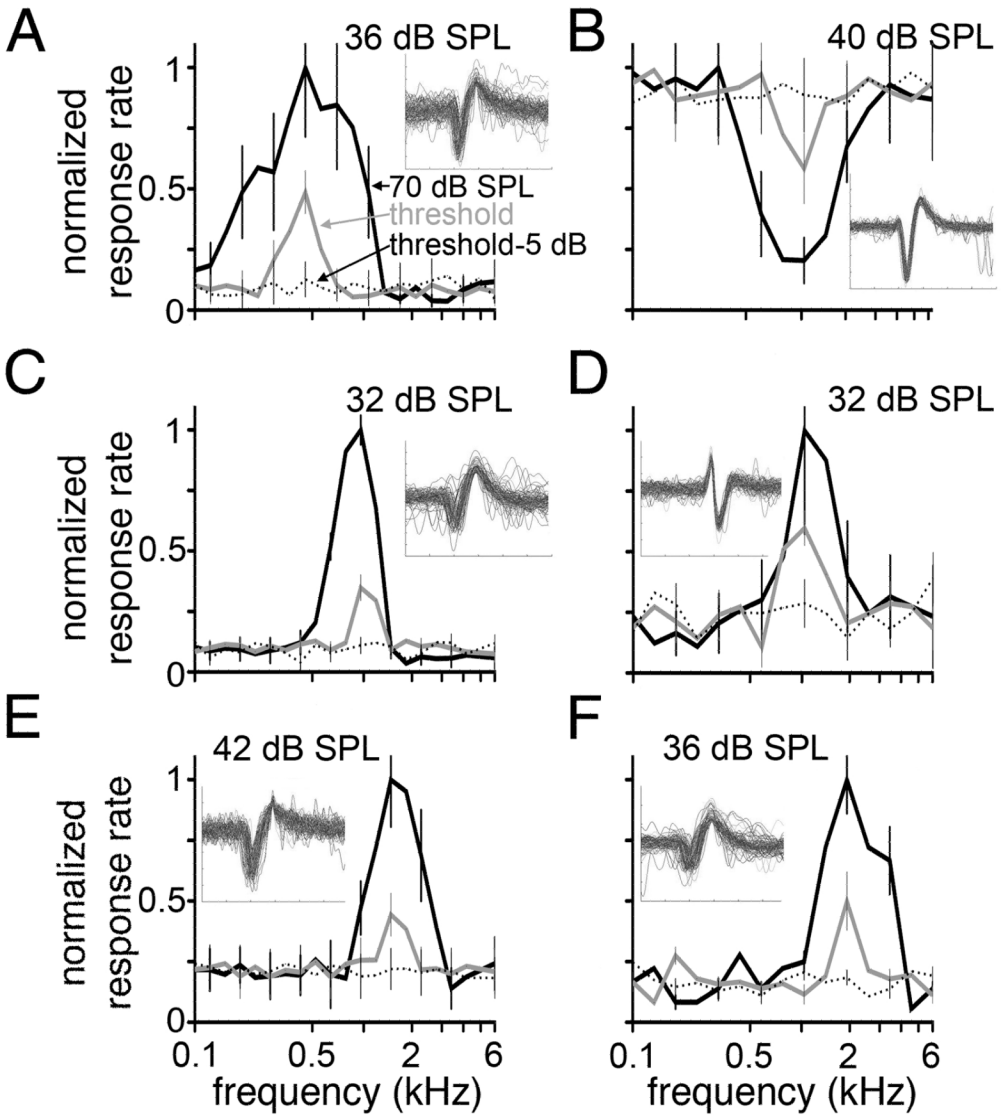

Fig. 1.

Normalized response to pure tones. Firing rate as a function of tone frequency is plotted for six units recorded in the SON. Response rates to pure tones (0.1–6 kHz) presented at 70 dB SPL (black solid lines), threshold (gray lines), and 5 dB below threshold (black dotted lines) are shown. Each function (A–F) was normalized to the maximum firing rate obtained at 70 dB SPL; 85, 77, 98, 132, 88, and 90 spikes/sec, respectively. Error bars represent SEM and are shown for alternating data points for clarity. Threshold is noted at the top of each panel. Insets show 6-msec voltage traces of 100 overlaid waveforms. For five units (A,C–F), a single frequency evoked the maximum firing rate at both 70 dB SPL and threshold; BF = 0.49, 0.96, 1.04, 1.45, and 2.0 kHz, respectively. One unit (B) exhibited frequency-specific inhibition. In this case, the BF (1.04 kHz) was defined as the frequency that induced the greatest inhibition of spontaneous rate. Units were recorded from the SON immediately preceding tracer injection.

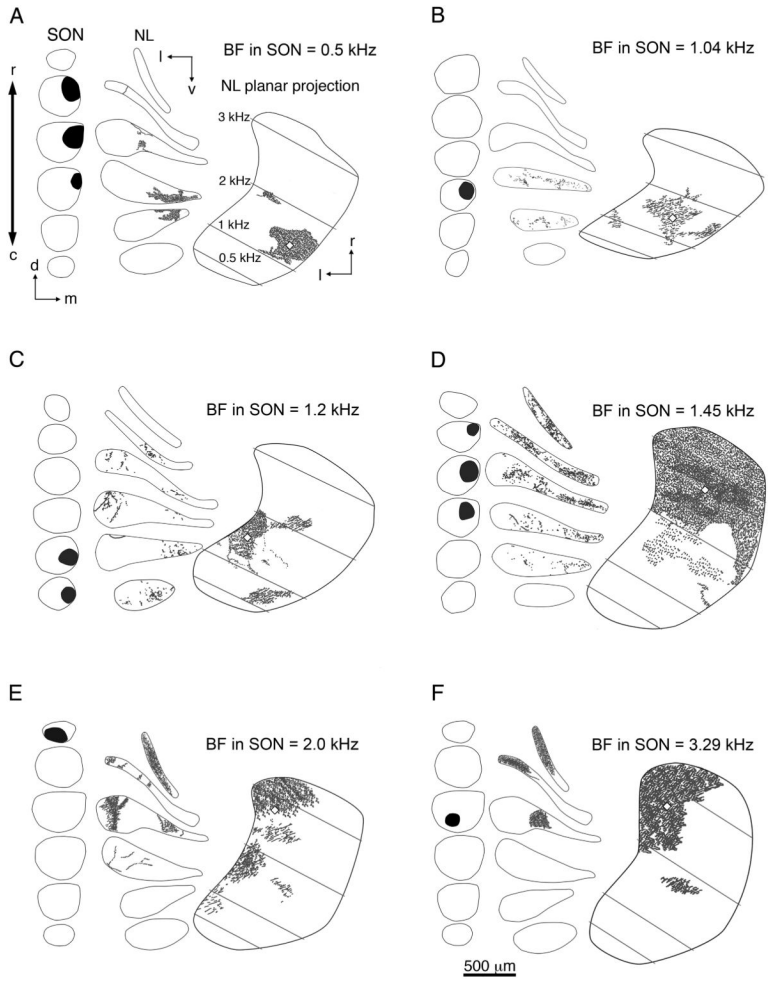

Fig. 2.

A–F: Line drawings depicting injection sites in SON of six representative cases that received a single injection and anterograde labeling in the ipsilateral NL. Within each panel, the location of the injection (black areas) is shown in serial coronal sections through SON arranged from rostral to caudal (left). The distribution of anterograde labeling in NL (gray dashes) is shown in a series of coronal sections through NL (center) and on horizontal planar projections of NL (right). Black lines indicate the border of SON or NL. White lozenges represent the centers of mass of the terminal fields (see Materials and Methods). Gray lines indicate isofrequency bands across NL. Characteristic frequencies (CF) were calculated as described by Rubel and Parks (1975) and listed in A. BFs of the injection sites are listed at the top right of each panel. Examples show injections localized to the rostral (E,F), caudal (B,C), lateral (F), medial (A–D), dorsal (A,B,D), or ventral (F) SON. Anterograde labeling was found in rostral (D–F) and caudal regions of NL (A,B). E: This case shows anterograde labeling across the majority of the tonotopic axis in NL. For this case, the center of mass was determined using all anterograde labeling except for the small satellite of labeled terminals located in the 1.5-kHz CF region of NL. The frequency response curves of B,D,E are shown in Figure 1B,E,F, respectively. NL, nucleus laminaris; SON, superior olivary nucleus; c, caudal; d, dorsal; l, lateral; m, medial; r, rostral; v, ventral. Scale bar = 500 μm.

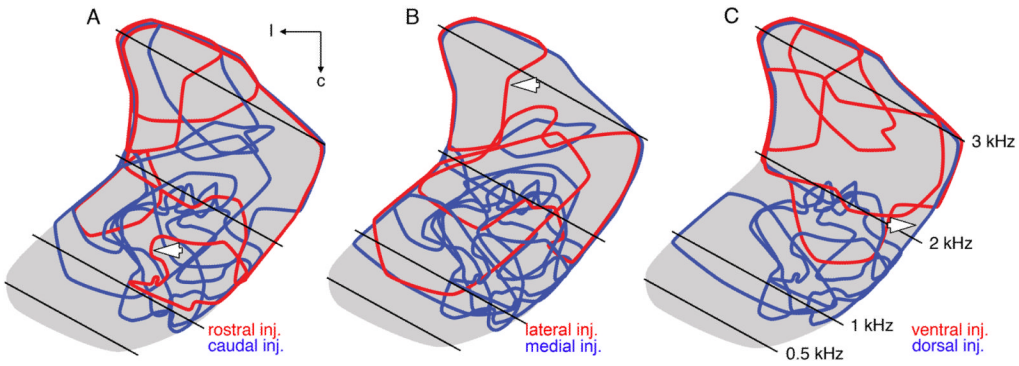

Fig. 3.

Comparative distribution of terminal fields in NL following injections into disparate halves of SON. Contours of labeled terminal fields superimposed onto a single horizontal planar projection of NL (gray). Calculated CFs of the isofrequency bands (black lines) are listed in C. A: Distribution of terminal fields arising from injections restricted to either the rostral (red contours; n = 4) or the caudal (blue contours; n = 7) SON. No apparent separation of blue and red contours suggests no topography between the rostrocaudal axis of SON and anterograde labeling in NL. White arrow indicates red contour of terminal field illustrated in Figure 2A. B: Red and blue contours represent terminal fields following injections into lateral (n = 3) and medial (n = 8) SON, respectively. The red and blue contours overlap, suggesting no topography between the mediolateral axis of SON and anterograde terminal fields in NL. Arrow indicates red contour of terminal field illustrated in Figure 2F. C: Terminal fields from injections into dorsal (blue contours; n = 5) or ventral (red contours; n = 4) SON appear reasonably well segregated, suggesting a topographic projection from the dorsal SON to caudal NL and from the ventral SON to rostral NL. Arrow indicates blue contour of the terminal field illustrated in Figure 2D. NL, nucleus laminaris; SON, superior olivary nucleus; c, caudal; l, lateral.

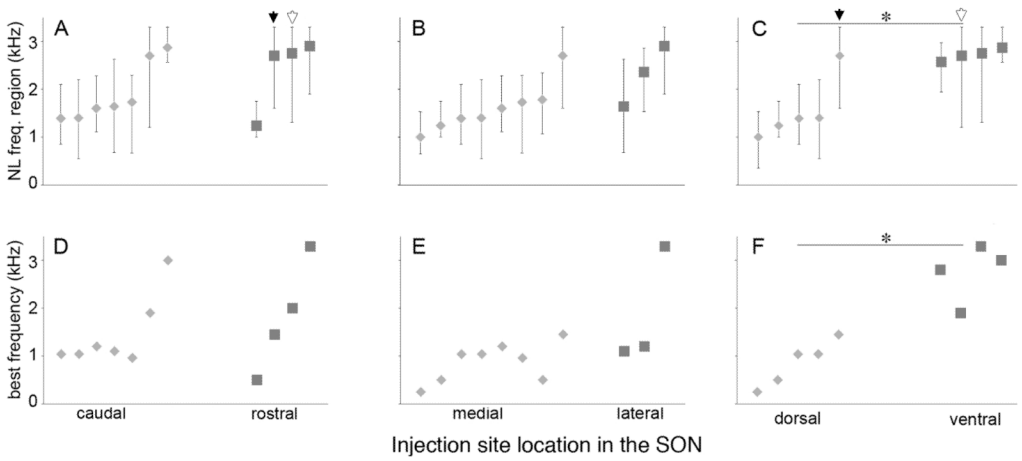

Fig. 4.

Topography of SON projections to NL. Cases are aligned along the abscissa by CF at the center of labeled terminal field in NL. A–C: Extent of terminal fields across the frequency axis in NL. Lozenges and squares indicate tonotopic position of the centers of mass of the terminal fields (see Materials and Methods). Bars represent the frequency range of NL innervated by labeled SON axons. A: Cases with tracer injections localized to caudal (lozenges; n = 7) and rostral (squares; n = 4) SON. NL frequencies at the center of terminal fields were not different between rostral and caudal groups (P = 0.53). Black and white arrows indicate two cases with axonal labeling covering greater than half of the area of NL. B: Cases with medial (lozenges; n = 8) and lateral (squares; n = 3) injection sites. NL frequencies at the center of terminal fields were not different between medial and lateral groups (P = 0.50). C: Cases with injections into dorsal (lozenges; n = 5) and ventral (squares, n = 4) SON. Projections from the dorsal SON innervated a lower frequency region of NL than projections from the ventral SON (P = 0.032). D–F: Lozenges and squares designate BFs at injection sites in SON. D: BFs of caudal injection sites (lozenges) and rostral injection sites (squares) were not significantly different (P = 0.53). E: BFs of medial (lozenges) and lateral (squares) injection sites were not significantly different (P = 0.085). F: BFs of dorsal (lozenges) injection sites were significantly lower than that of ventral (squares) injections (P = 0.016).

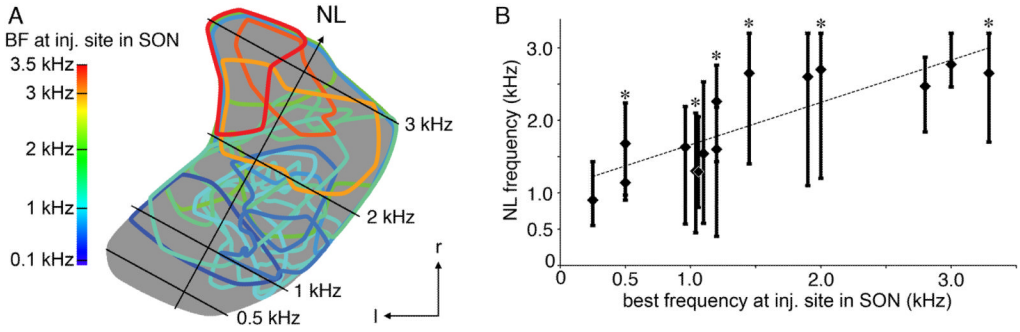

Fig. 5.

Tonotopic projections of the SON to NL. A: Planar projection of NL illustrating tonotopic organization of SON projection to NL. Calculated CFs of isofrequency bands (lines) and the tonotopic axis of NL (arrow) are shown. Distribution of SON terminal fields (n = 15 animals) mapped onto a single planar projection of NL (gray). The color of the contours represents the BF recorded at the injection site in SON using a color scale (left). B: Tonotopic position of labeled terminal fields in NL correlates with BF recorded at injection site in SON ($r2 = 0.68$, $P < 0.001$, $n = 15$). For each case, the BF at the injection site is plotted against the CF of NL innervated by anterogradely labeled terminals. Lozenges indicate the CF of NL at the center of mass of the terminal field; bars indicate the CF range of NL innervated by the terminal field. For one of the two cases with BF = 1.04 kHz, the BF is slightly offset to 1.06 kHz and the center lozenge is outlined in white for visualization. Asterisks identify cases illustrated in Figure 2. NL, nucleus laminaris; SON, superior olivary nucleus; l, lateral; r, rostral.

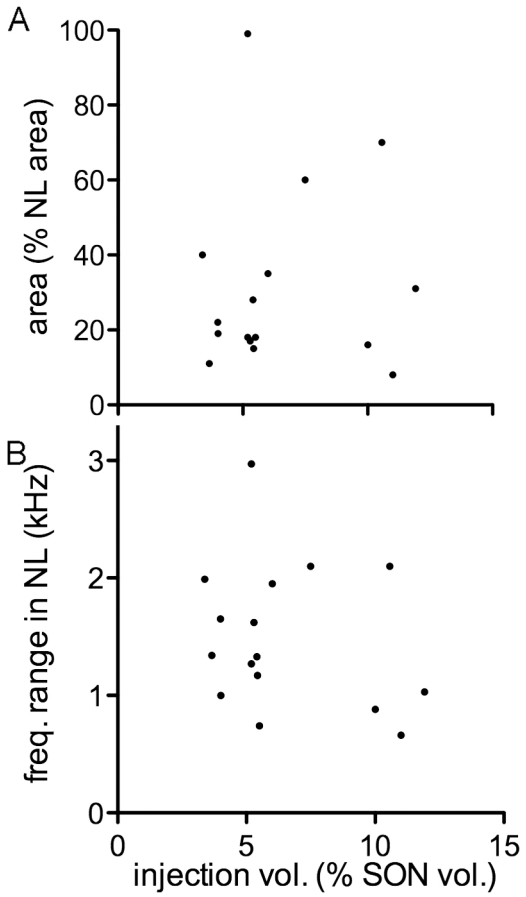

Fig. 6.

Size of the injection site in SON is not correlated with area and frequency range of labeled terminal fields in NL. The injection size ranged from 4% to 12% (6.5% ± 2.8%) of the volume of the SON. A:The size of the injection site was not correlated with the percentage of NL innervated by the labeled terminal field ($r^2 = 0.006$, $P = 0.79$, $n = 16$). The innervated area of NL ranged from 8% to 99% (31% ± 24%). B: The size of the injection site in SON was not correlated with the frequency range of NL innervated by labeled axons ($r^2 = 0.059$, $P = 0.36$, $n = 16$).

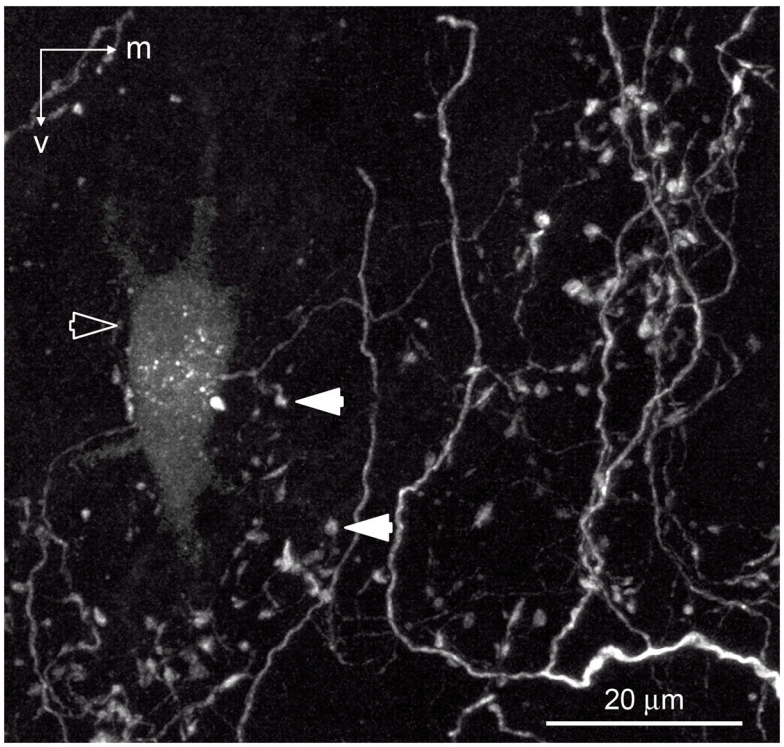

Fig. 7.
Intermediate CF region of NL (between 1 and 2.5 kHz) showing a retrogradely labeled NL neuron (open arrow) surrounded by labeled SON axons (white; examples indicated with solid white arrowh). m, Medial; v, ventral. Scale bar = 20 μm.

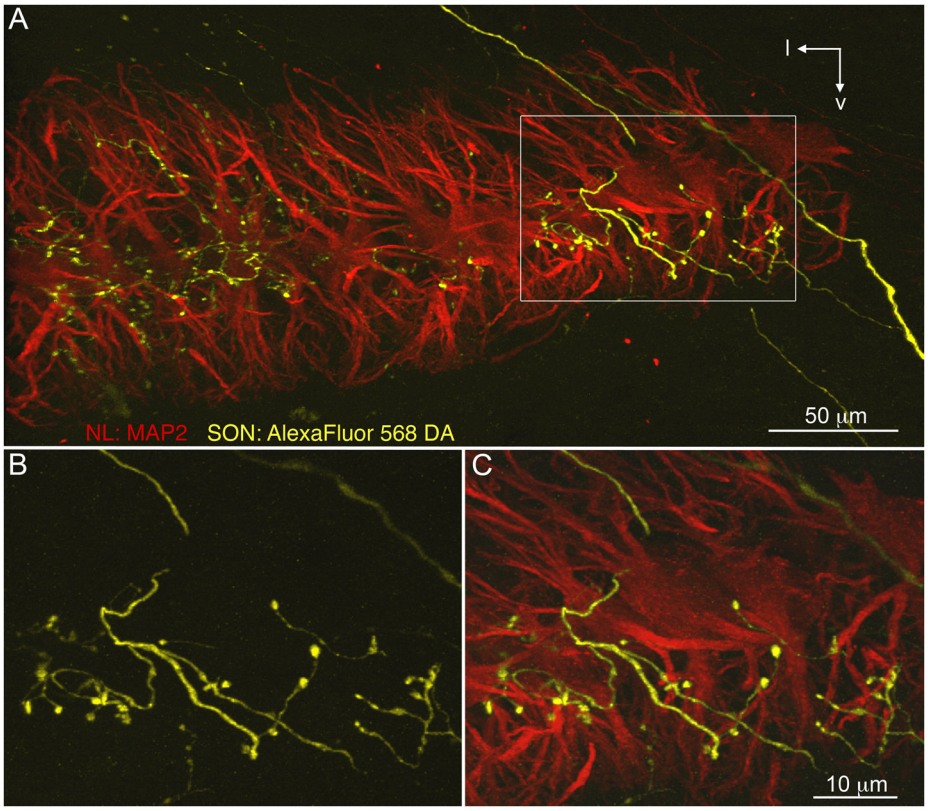

Fig. 8.

SON axonal arborizations in NL. SON axons visualized with AlexaFluor 568 dextran amine (yellow) innervate NL. MAP2 immunoreactivity (red) reveals the dendrites and cell bodies of NL neurons. A: Fine SON axon branches with bouton-like swellings on all laminae. White rectangle shows location of the magnified images in B,C. B: Magnified image of the SON axon that entered NL dorsally, branched, and formed large varicosities. C: Immunostaining for MAP2 shows this SON axon branch formed varicosities on cell bodies and ventral dendrites of NL. l, Lateral; v, ventral. Scale bars = 50 μm in A; 10 μm in C (applies to B,C).

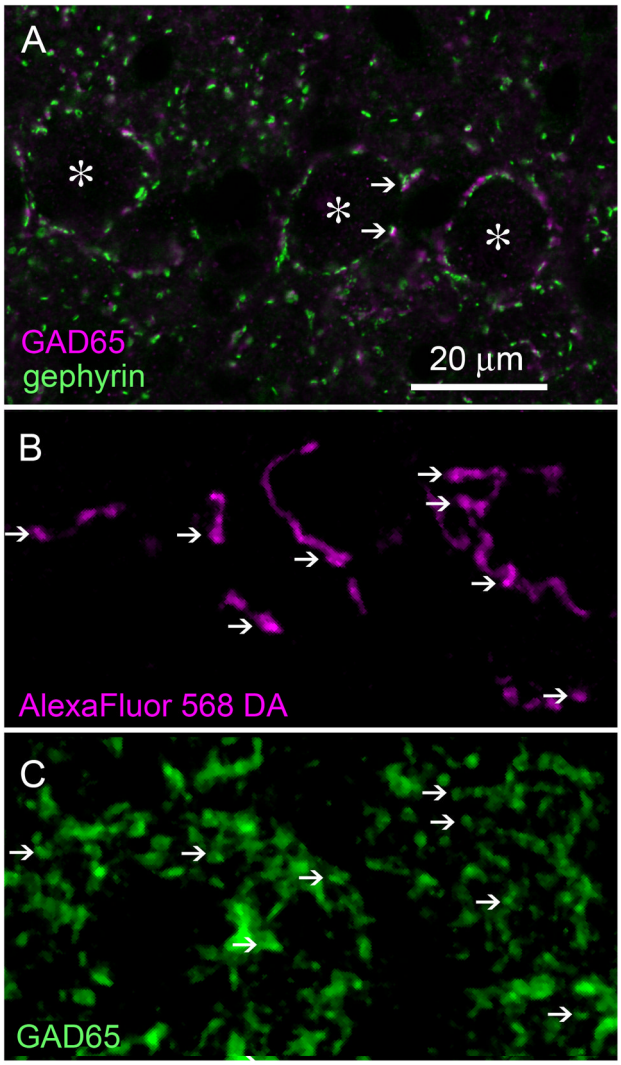

Fig. 9.

SON axonal swellings in NL are GABAergic. A:GAD65 immunolabeling (magenta) of GABAergic presynaptic site and gephyrin immunolabeling (green) of inhibitory postsynaptic sites are colocalized in NL (examples, arrows). Asterisks indicate NL cell bodies. B: Single plane confocal image of NL showing SON axons labeled with AlexaFluor 568 dextran amine (magenta). Arrows indicate locations of varicosities. C: GAD65 immunolabeling (green) in NL. D: Combined channel image shows labeled axonal varicosities colocalized with GAD65 puncta (white). E:High-magnification images. Combined channel image shows labeled axonal varicosities colocalized with GAD65 immunoreactivity (left; arrowheads). AlexaFluor 568 dextran amine (center; magenta) and GAD65 (right; green) labeling are shown separately. F:Combined channel image with the GAD65 image rotated 90° clockwise. The GAD65 puncta (green) show sparse colocalization with fluorescent tracer (magenta). Image taken from the cell body lamina in the intermediate region of NL. Scale bars = 20 μm in A; 3 μm in E; 10 μm in F (applies to B–D,F).

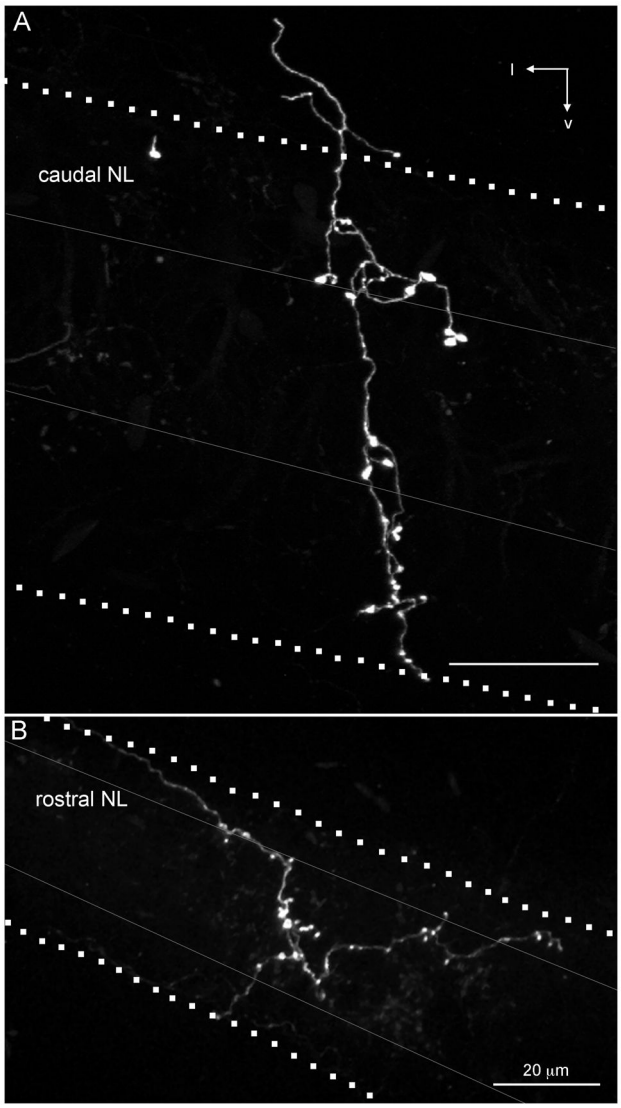

Fig. 10.

SON axonal branches ramifying in high-CF and low-CF regions in NL. AlexaFluor 568 dextran amine labeled SON axons (white) extending across all laminae of NL. In both examples, the axon branch enters NL from the dorsolateral brainstem; however, we observed axons entering NL from both the dorsal and ventral sides. Dotted lines indicate the boundaries of NL, gray lines indicate boundaries of cell body lamina within NL. A:Rostral, high-CF region of NL innervated by an SON axonal arbor. Image is a maximum intensity projection through a 200-μm-thick optical stack. B: Caudal, low-CF region of NL innervated by an SON axonal arbor. Image is a maximum intensity projection through a 300-μm-thick optical stack. l, Lateral; v, ventral. Scale bars = 20 μm.

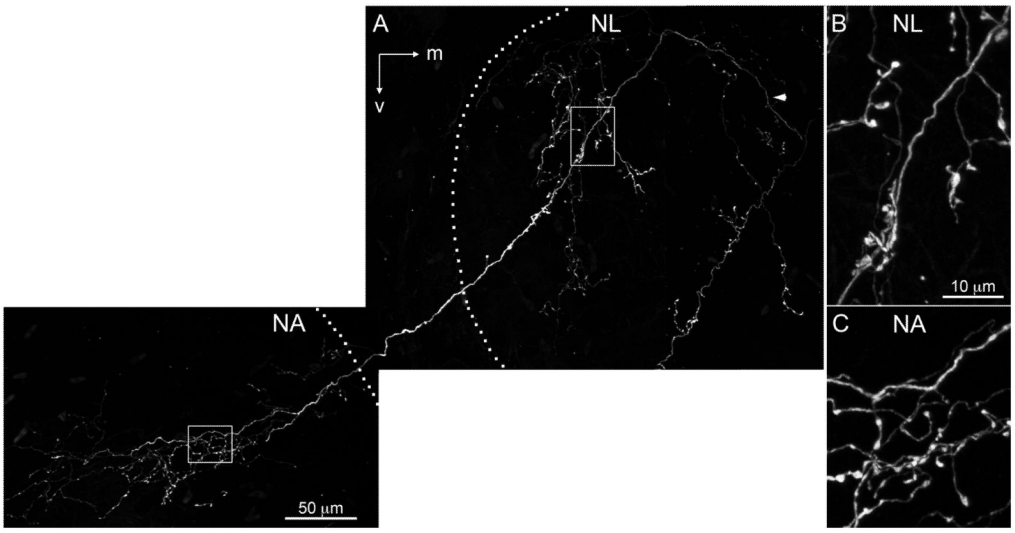

Fig. 11.

SON axonal arborization innervating multiple auditory nuclei. A: Labeled SON axon (white) coursed dorsolateral through NL (arrowhead) and turned ventrolateral, forming branches and bouton-like swellings in the lateral NL, then innervated nucleus angularis (NA). Borders of the nuclei are indicated with dotted lines. Rectangles show location of magnified images in B,C. B: Magnified image of the labeled SON axonal arbor within NL. C:Magnified image of the labeled SON axonal arbor within NA. NA, nucleus angularis; NL, nucleus laminaris; m, medial; v, ventral. Scale bars = 50 μm in A; 10 μm in B (applies to B,C).

TABLE 1

Primary Antibodies Used

Antigen	Immunogen	Manufacturer, species in which antibody was raised; mono- vs. polyclonal; catalog No.; lot No.	Dilution used
Microtubulin-associated protein 2 (MAP2)	Bovine brain MAP2 (aa 997–1332)	Chemicon; mouse; monoclonal; clone AP20; MAB3418; lot LV1486526	1:1,000
Glutamate decarboxylase 65 (GAD65)	Human GAD65 from baculovirus-infected cells	Millipore; rabbit; polyclonal; AB5082; lot LV1580833	1:1,000
Gephyrin	Purified rat gephyrin	Synaptic Systems; mouse; monoclonal, clone mAB7a; 47011; lot 147011/21	1:1,000